Noise Resilient QR code Zero-watermarking System in Contourlet-SVD and SVD Domains for Improved Teleradiology

[1] Velumani R and [2] Seenivasagam V

[1]Associate Professor, Department of Information Technology, Sethu Institute of Technology, Pulloor, Kariapatti-India, 626115. Phone: +91 9865768480 Fax: +91 04566 308000
velumaniramesh@yahoo.com
[2]Professor, Department of Computer Science and Engineering, National Engineering College, Kovilpatti-India, 628503.

Abstract: Patient authentication and protection of patient data are the major concerns in teleradiology environments. Clinical observations at referral sites can help the remote radiologist make thorough interpretations. Further, fidelity of the host images must be preserved for accurate readings. In this paper, we present a zero-watermarking scheme to resolve these issues. A Health Level 7 message comprising Patient I Dentification and Observation segments encoded as Quick Response code is taken to be a watermark. The system is implemented in the SVD and Contourlet-SVD domains employing the Hu's invariants to achieve robustness. We analyze the performance of the system in both the domains exclusively under noise attacks and conclude that CT-SVD domain offers better robustness. Our experimental results show that lower order Hu's moments are adequate to impart robustness in zero-watermarking systems. The paper also addresses the need to identify invariants resilient to noise for medical images with small regions of interest.

[Velumani R and Seenivasagam V. **Noise Resilient QR code Zero-watermarking System in Contourlet-SVD and SVD Domains for Improved Teleradiology.** *Life Sci J* 2018;15(7):87-99]. ISSN: 1097-8135 (Print) / ISSN: 2372-613X (Online). http://www.lifesciencesite.com. 12. doi:10.7537/marslsj150718.12.

Keywords: zero-watermarking, Hu's moments, Contourlet, SVD, QR code, HL 7, Teleradiology

1. Introduction

Healthcare providers adopt teleradiology services under shortage of in-house radiologists and lack of provisions for subspecialty readings (Benjamin et al, 2010). Standards on teleradiology demand positive patient identification, provision of past medical history etc., to the reading site (Benvon Cramer, 2008). Legislative standards such as Health Insurance Portability and Accountability Act (HIPAA,) define stringent requirements on patient data security and privacy (US Department of Health and Human Services). An extensive study (Nyeem et al, 2012) on applying watermarking in teleradiology presented advocates the need for designing multiple watermarking systems to address the security and privacy needs in teleradiology. In this paper, we present a QR (Densowave) code based zero-watermarking (Chang et al, 1999) system for positive patient identification and to deliver clinical observations to the remote radiologist. In zero-watermarking, during embedding, a binary pattern generated out of the essential characteristics of the host image is combined with the watermark image to generate a secret key. At the receiving end, on extraction, the same procedure is applied to create a binary pattern which is combined with the secret key to construct the watermark image. Zero-watermarking schemes in the literature are based on Visual Secret Sharing (VSS) which is a combination of Visual Cryptography (VC) (Naor and Shamir, 1995) and generalized secret sharing (Guo and Georganas, 2003). Secret sharing refers to the distribution of a secret image as multiple shares and combining the shares to construct the secret image. VC defines a set of rules to represent white and black pixels and reveals the secret image by physically superimposing the transparencies of the Secret Shares without any computations.

In VSS based zero-watermarking (Chang and Chuang, 2002) schemes, a Master Share is constructed from the essential image features and it is combined with the watermark image to generate a Secret Share at the sender's side. Similarly, a Master Share is generated from the host image and is combined with the Secret Share to reveal the watermark at the receiver's end. Image moments (Prokop and Reeves, 1992) find wide applications in pattern recognition, object classification and image reconstruction. Many authors have testified the invariant nature of image moments, by employing them in watermarking schemes to achieve robustness against geometric attacks. However, their robustness has not been extensively studied under the influence of noise. Medical images are corrupted by noise during acquisition and transmission resulting in obvious visual degradations. In this paper, we propose a zero-watermarking system robust to noise by employing the invariants to construct the Master Share. From literature on classical watermarking systems, we

understand that transform domain based systems provide better robustness compared to that of spatial domain. The system is implemented in the composite Contourlet -Singular Value Decomposition (CT-SVD) and SVD domains to enhance the intactness of the Master Shares. We have tested the systems with medical images of different modalities and a binary QR code watermark generated from a Health Level7 (HL7) (Corepoint Health) message segment.

We have investigated the robustness of the invariants and in turn the proposed system in both the domains, under noise attacks by evaluating the readability of the watermarks constructed from the noisy images. In this paper, we deal with four most predominant noise types such as AWGN (Additive White Gaussian Noise), poisson noise, salt and pepper noise and speckle noise. The rest of the paper is organized as follows. In section 2, we present a background on the underlying fundamentals and mathematical concepts related to the implementation of our work. The characteristics of the noise types considered in this paper are presented in section 3.

The proposed system is described in Section 4 and experimental results and comparisons are given in Section 5. Discussion on the results is presented in section 6. The paper is concluded in section 7.

2. Background

2.1 QR Codes in Healthcare

Healthcare institutions resort to patient wristbands displaying QR codes, encoded with patient identifiable data to manage front office and clinical procedures. The structure of the QR code is shown in Figure 1. An overview on QR codes and their applications is elaborately discussed in an article by Tan Jin Soon (2008). The application of 1D, 2D barcodes, Radio Frequency Identification (RFID) tags and QR codes for automatic patient identification has been studied by García-Betances and Huerta (2012). The authors advocate the use of QR codes for patient identification in low budgeted health centers, due to their simplicity and ubiquity of smart phones enabled with QR code readers. Further, web links to essential patient information are encoded into QR codes for instant access by paramedics under emergency (Kerry Davis, 2012). Chen and Wang (2009) proposed a blind watermarking scheme to embed a QR code and a facial image in the DCT coefficients of a medical image. Another blind watermarking scheme to embed a QR code of the Universal Content Identifier (UCI) for authentication of multimedia content is proposed by Kim et al (2010). This scheme embeds a 64x64 QR code into the spatial, DCT and FFT domains of a digital image of size 512x512.

2.2 Integration of HL7 and Teleradiology

HL7 protocol provides standards for interoperability between disparate healthcare providers and stakeholders for exchange, integration and retrieval of electronic health information. It comprises of a collection of message types to handle different events. Each message type consists of a number of segments which carry the message. The Patient I Dentification (PID) and Observation (OBX) segments contain patient identification and observation data respectively. A sample HL7 message with PID, OBX and other related segments, is shown in Figure 2. In teleradiology, images are represented in Digital Imaging and Communications in Medicine (DICOM) formats. The need to integrate DICOM and HL7 as a single protocol to improve the workflow is addressed by Cordos et al (2010).

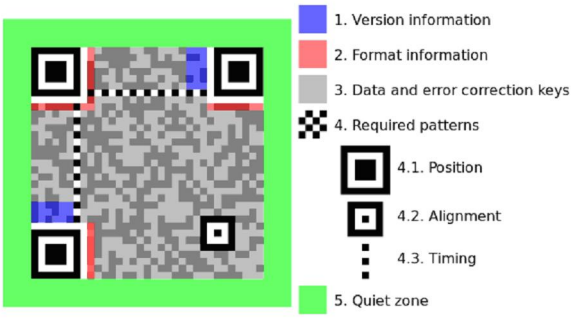

Figure 1. Structure of QR Code

```
MSH|^~\&|LCS|LCA|LIS|TEST9999|199807311532||ORU^R01|3630|P|2.2
PID|3|2161348473|20923085580|01572633|20923085580^TESTPAT||19730204|
M|||^^^^00000-0000||||||86427531^^^03|SSN‡                          HERE
PV1||I|^802^1||||8625^Physician^Michael|86-7468^||xxx|||||||V1001
ORC|NW|8642753100013^LIS|20923085580^LCS|||||199807280000000|||PEED
OBR|1|8642753100013^LIS|20923085580^LCS|083824^PANEL
083824^L|||199807280836000||||||
CH13380|19980728000000||||||20923085580||199807300418000|||F
OBX|1|NM|150001^HIV-1            ABS-O.D.              RATIO^L|||||||N|X
OBX|2|CE|001719^HIV-1       ABS,       SEMI-QN^L||HTN|||||N|F|19910123||
19980729155700|BN
NTE|1|L|Result:          NEGATIVE          by          EIA          screen.
NTE|2|L|No          antibodies          to          HIV-1          detected.
OBX|3|CE|169999^.^L||SPRCS|||||N|F|||19980728130600|BN
NTE|1|L|NOTE:               Submission               of               serum
NTE|2|L|separator                    tube                    recommended
NTE|3|L|for          this          test.          Thank          you
NTE|4|L|for          your          cooperation          if          you
NTE|5|L|are               already               doing               so.
OBX|4|CE|169998^.^L||SPRCS|||||N|F|||19980728130600|BN
ZPS|1|BN|LABCORP                    HOLDINGS|1447                    YORK
COURT^^BURLINGTON^NC^272152230|8007624344
```

Figure 2. Sample HL7 message

2.3 Contourlet Transform

Do and Vetterli (2005), proposed the Contourlet Transform (CT) which combines Laplacian Pyramid (LP) and Directional Filter Bank (DFB) structure. The framework for Contourlet decomposition is given in Figure 3. It provides directionality and anisotropy properties in addition to multiscale and time-frequency localization proprieties of wavelets. This transform provides the best approximation of smooth contours and edges of the image subjected to decomposition. Many authors have implemented blind and non blind watermarking algorithms in the Contourlet domain

(Salahi et al, 2008; Shu et al, 2008; Song et al, 2008). On applying CT on an image *I*, at each level *j* of contourlet decomposition, a lowpass image I_j is generated at the LP stage. At the DFB stage, a set of band pass images B_j, j=1,2,…2^k, where *k* is the number of directional decompositions at each level are generated. While the lowpass image preserves the Low Frequency (LF) components, directional subbands preserve the high frequency components. This process may be repeated for the desired level of decomposition with the lowpass image.

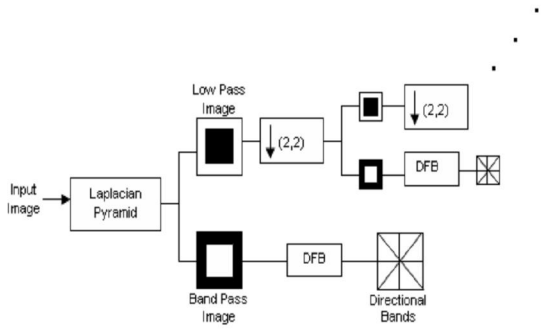

Figure 3. Contourlet Decomposition

2.4 Singular Value Decomposition

Singular Value Decomposition is a linear algebraic tool widely used in factorization and approximation of matrices. For any $n \times n$ real or complex matrix *A*, SVD is a factorization of the form given in (1) where *S* is a $n \times n$ diagonal matrix with nonnegative real numbers on the diagonal; *U* and *V* are the unitary matrices of the order $n \times n$.

$$[U, S, V] = SVD(A) \tag{1}$$

The diagonal entries S_{ii} of *S* are known as the Singular Values (SV) of *A*. The columns of *U* and *V* are called as left-singular vectors and right-singular vectors of *A* respectively. Matrix *A* can be reconstructed from the singular and unitary matrices as shown in (2) where *V'* is the complex conjugate of *V*.

$$A = U * S * V' \tag{2}$$

The singular values of *S* are invariant to transpose, flipping, scaling, rotation and translation. Further, best approximation of an image can be realized with only a few significant singular values. The composite CT-SVD domain provides better robustness to different classes of attacks. A zero-watermarking scheme proposed by Zeng and Zhou (2008) embeds the watermark in the largest SVs of the non overlapping blocks of the LF subband in the Contourlet domain. This scheme is reported to be robust against attacks such as added noise, JPEG compression and cropping.

2.5 SVD and VSS Based Zero-watermarking

Zero-watermarking schemes based on Visual Cryptography (VC) and SVD are proposed in many papers. Hsu and Hou (2005) proposed a scheme in which the Master Share is created from the distribution of means in the host image for a normal population. Wang and Chen (2009) proposed a scheme in the composite DWT_SVD domain in which, the Master Share is created from the SVs of the non overlapping blocks of the LL subband. A hybrid scheme proposed by Rawat and Raman (2012) is based on Fractional Fourier Transform (FrFT) and SVD. Initially, a subimage is created from selected non overlapping blocks of the host image. The Master Share is created from the image features extracted by applying FrFT and SVD on the subimage.

The Secret Share is generated from the Master Share and the secret watermark image. A VSS based zero-watermarking scheme, proposed by Fan et al. (2012), employs the Bose–Chaudhuri–Hocquenghem (BCH) code for error correction. An image comprising only selected Most Significant Bit (MSB) planes of the host image is transformed by DWT. A secret key is used to select coefficients of the LL subband to create the Master Share. The Secret Share is created from the quantized host image, Master Share and the scrambled watermark. The last two schemes are reported to be resilient to both geometric and non geometric attacks.

2.6 Theory and Applications of Hu's Moments

Statistical moments find extensive applications in pattern recognition, in object identification and classification. Moments are invariant pattern features used to discriminate the objects under distortions. According to Hu (1962), image patterns can be represented by their geometric moments. The 2D moment of order $(p+q)$ of a digital image $f(x,y)$ of size *MxN* is defined as

$$m_{pq} = \sum_{x=0}^{M-1} \sum_{y=0}^{N-1} x^p y^q f(x, y) \tag{3}$$

Where $p=0,1,2...M-1$. and $q=0,1,2,...N-1$ are integers. The corresponding central moment of order $(p+q)$ is defined as

$$\mu_{pq} = \sum_{x=0}^{M-1} \sum_{y=0}^{N-1} (x - \bar{x})^p (y - \bar{y})^q f(x, y) \tag{4}$$

for $p = 0,1,2....M-1$ and $q=0,1,2,...N-1$.

$$\bar{x} = \frac{m_{10}}{m_{00}} \quad \text{and} \quad \bar{y} = \frac{m_{01}}{m_{00}} \tag{5}$$

where

The normalized central moment of order $(p+q)$ is defined as

$$\eta_{pq} = \frac{\mu_{pq}}{\mu^{\gamma}_{00}} \tag{6}$$

$$\gamma = \frac{p+q}{2} + 1$$

where for $p+q = 2,3,\ldots$ (7)

From the above equations, the 2D moments invariant to translation, scaling, rotation and mirroring are derived as below.

$$I_1 = \eta_{20} + \eta_{02} \quad (8)$$

$$I_2 = (\eta_{20} - \eta_{02})^2 + 4\eta_{11}^2 \quad (9)$$

$$I_3 = (\eta_{30} - 3\eta_{12})^2 + (3\eta_{21} - \eta_{03})^2 \quad (10)$$

$$I_4 = (\eta_{30} + \eta_{12})^2 + (\eta_{21} + \eta_{03})^2 \quad (11)$$

$$I_5 = (\eta_{30} - 3\eta_{12})(\eta_{30} + \eta_{12})[(\eta_{30} + \eta_{12})^2 - 3(\eta_{21} + \eta_{03})^2] + (3\eta_{21} + \eta_{03})(\eta_{21} + \eta_{03})[3(\eta_{30} + \eta_{12})^2 - (\eta_{21} + \eta_{03})^2] \quad (12)$$

$$I_6 = (\eta_{20} - \eta_{02})[(\eta_{30} + \eta_{12})^2 - (\eta_{21} + \eta_{03})^2] + 4\eta_{11}(\eta_{30} + \eta_{12})(\eta_{21} + \eta_{03}) \quad (13)$$

$$I_7 = (3\eta_{21} - \eta_{03})(\eta_{30} + \eta_{12})[(\eta_{30} + \eta_{12})^2 - 3(\eta_{21} + \eta_{03})^2] + (3\eta_{12} - \eta_{30})(\eta_{21} + \eta_{03})[3(\eta_{30} + \eta_{12})^2 - (\eta_{21} + \eta_{03})^2] \quad (14)$$

Of the above, I_1 to I_6 are called translation, scaling and rotation invariants. I_7 whose sign changes to distinguish mirrored images is called the skew invariant. Hu demonstrated the invariant nature of these moments in recognizing printed uppercase characters. From equations (8) to (14), it is evident that the computational complexity is high for higher order moments. From literature, we understand that the higher order moments are sensitive to noise. An analysis on Hu's moments (Huang and Leng, 2010) says that the moment invariants change on scaling and rotation and fluctuation of moments decreases as spatial resolution increases. Further, it is also identified that there is no obvious decrease in fluctuation when the resolution goes above a threshold. Hu's moments find applications in designing watermarking systems robust to geometric attacks. Alghoniemy and Tewfik (2000; 2004) studied the invariance properties of image moments and generated invariant watermarks from the Hu's geometric moments to achieve robustness against geometric attacks. Similarly, a watermarking algorithm for copyright protection of semantic content in a video (Tzouveli, 2006) generates the invariant watermark from the entire set of weighted Hu's moments of the video object. In a recent paper, an invisible watermarking scheme based on four lower order Hu's moments is proposed; it is found to be superior to a Fast Fourier Transform (FFT) based technique presented in the same paper under geometric and noise attacks (Mahbuba et al, 2012).

2.7 Arnold Transform

The Arnold Transform is a periodic chaotic transform that maps any coordinate position (x,y) to (x_n,y_n) and vice-versa in any nxn space as shown in equations (15) and (16). Chaotic transforms are commonly employed in watermarking systems to scramble the watermarks before embedding and to recover the same on extraction.

$$\begin{bmatrix} x_n \\ y_n \end{bmatrix} = \begin{bmatrix} 1 & 1 \\ 1 & 2 \end{bmatrix} \begin{bmatrix} x \\ y \end{bmatrix} \pmod{n} \quad (15)$$

$$\begin{bmatrix} x \\ y \end{bmatrix} = \begin{bmatrix} 1 & 1 \\ 1 & 2 \end{bmatrix} \begin{bmatrix} x_n \\ y_n \end{bmatrix} \pmod{n} \quad (16)$$

We understand from (15) and (16) that both the Arnold Transform and its inverse are the same. The periodic and area preserving properties of this transform are suitable for realizing synchronization in watermarking systems. Recent medical image watermarking algorithms employ this transform for scrambling the watermarks (Li, 2012; Liu, 2012).

3. Noise in Medical Images

Artifacts are introduced into medical images due to noise generated on image acquisition, compression and transmission. Gaussian and non gaussian noises with different regularization models occur in medical images. Most works in the literature deal with AWGN (Lal, 2011). AWGN is a white noise added to the image by the transmission channel, that follows a gaussian distribution and constant spectral density. In an image contaminated with AWGN, value of each pixel is the sum of the actual pixel value and a random noise value with gaussian distribution. Poisson or photo counting noise is predominant in Positron Emission Tomography (PET) and fluorescence microscopy. The noise is characteristic of the image itself and is not influenced by any external sources.

In the noisy PET images degraded by poisson noise, the random variables follow a poisson distribution. Salt and Pepper noise appears as sparse black and white dots in a corrupted image. It is an impulse noise caused by the malfunctions in the capturing device and synchronization errors during digitization and transmission. Speckle noise is a multiplicative noise that appears as granular patterns commonly in ultrasound images. It is introduced due to scattering effects, increasing the mean gray level in the local area of the image. One can understand the characteristics of poisson and speckle noises from the

thesis by Sawatzky (2011). A brief account on the above noise types and the corresponding Probability Density Functions is given in (Gonzalez and Woods, 2005).

4. Proposed System

In this section, we present the algorithms for implementing the watermarking system in the hybrid CT-SVD domains. The phases of watermark creation, Master and Secret Share creation and watermark construction are covered in subsections with algorithms and illustrations. We have not given the algorithms exclusively for the SVD domain as they can be understood from the ones for CT-SVD domain.

4.1 Watermark Creation

We have encoded the HL7 message shown in Figure 2. into a QR code with open source Zebra Crossing (Zxing) software. We have set the QR code size to be medium, error correction level to be large and Unicode Set Transformation Format-8 (UTF-8) as the encoding standard with the Zxing User Interface. The resultant QR code is of size 230x230x3. We represent it as binary and consider only the inner region of size 109x109 for watermarking, excluding the quiet zone to reduce the computational complexity. The generated QR code and its trimmed form are shown in Figure 4(a) and Figure 4(b) respectively.

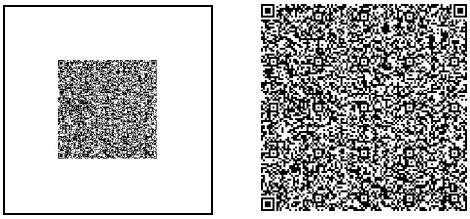

(a) (b)

Figure 4. Watermark Image (a) Actual Watermark (b) Trimmed Watermark

4.2. Secret Share Creation

Here, we present the procedure for Secret Share creation in the CT-SVD domain in Algorithm 1.

This algorithm is illustrated in Figure 5.

4.3 Watermark Construction

In this section, we present the procedure for Watermark Construction in the CT-SVD domain in Algorithm 2. This algorithm is illustrated with Figure 6. From the illustrations, we can see that the embedding and extraction algorithms follow the same procedure for Master Share creation. For system implementation in SVD domain the algorithms begin with block partitioning on the host image.

Algorithm.1: Master Share and Secret Share creation-CT-SVD

Input: *Host Image* ***H*** *of size* ***NxN****, Watermark* ***W*** *of size* ***mxm****, Key* (k_i,k_j) *for initial block Selection, size of block* ***bxb,*** *Number of iterations* ***i*** *for Arnold Transform*

Output: *Secret Share* ***Sshare*** *of size* ***mxm***

Step1. Apply Contourlet Transform on ***H*** *to generate a*
*****nxn*** *LF subband*
Step2. Perform ***bxb*** *block partitioning on the LF subband to generate* ***n/bxn/b*** *non overlapping*
blocks
Step3. Apply Arnold Transform on ***W*** *to generate scrambled watermark* ***SW***
Step4. Perform steps5-8 for each bit W_{ij} *of watermark*
Step5. Apply Arnold transform on (k_i,k_j) *to select a*
block from partitioned LF subband for Master
Share creation; Increment k_i *and* k_j *by* ***1***
Step6. Apply SVD to the selected block to generate ***U, S*** *and* ***V*** *matrices*
Step7. Compute the Hu's invariant moments I_1, I_2 *and* I_3 *for the diagonal matrix* ***S***
Step8. Create a 3 bit Master Share ***Mshare*** *out of the*
sign bits of I_1, I_2 *and* I_3
Step9. Perform XOR operation on ***Mshare*** *and*
SW *to generate Secret Share* ***Sshare,*** *of size* ***mxm;*** *i.e.* ***Sshare****=XOR(****Mshare,SW****)*

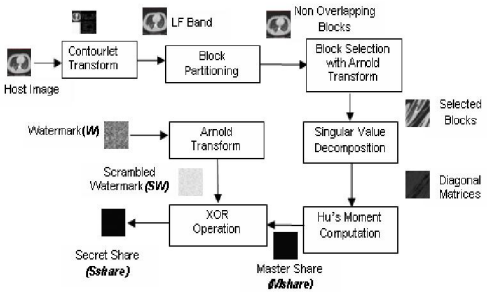

Figure 5. Secret Share Creation

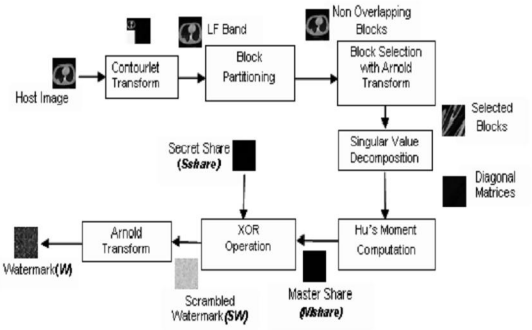

Figure 6. Watermark Construction

5. Experimental Results and Analysis

Algorithm 2: Watermark Construction-CT-SVD

Input: *Host image* ***H*** *of size* ***NxN,*** *Secret Share* ***Sshare*** *of size* ***mxm,*** *Key* ***(k_i,k_j)*** *for initial block Selection, size of block* ***bxb,*** *Number of iterations* ***i*** *for Arnold Transform*

Output: *Watermark* ***W*** *of size* ***mxm***

Step1. Apply Contourlet Transform on ***H*** *to generate a* ***nxn*** *LF subband*

Step2.Perform ***bxb*** *block partitioning on the LF subband to generate* ***n/bxn/b*** *non overlapping blocks*

Step3.Perform steps 4-8 for each element of ***Sshare***

Step4.Apply Arnold transform on ***(k_i,k_j)*** *to select a block from partitioned LF subband for Master Share creation; Increment* ***k_i*** *and* ***k_j*** *by 1*

Step5.Apply SVD to the selected block to generate ***U,S*** *and* ***V*** *matrices*

Step6.Compute the Hu's invariant moments ***I_1, I_2*** *and* ***I_3*** *for the diagonal matrix* ***S***

Step7.Create a 3 bit Master Share ***Mshare*** *out of the sign bits of* ***I_1,I_2*** *and* ***I_3***

Step8. Perform XOR operation on ***Mshare*** *and* ***Sshare*** *to get* ***SW;*** *i.e.* ***SW=XOR(Mshare, Sshare)***

Step9.Apply Arnold transform to unscramble ***SW*** *to get* ***W***

a

b

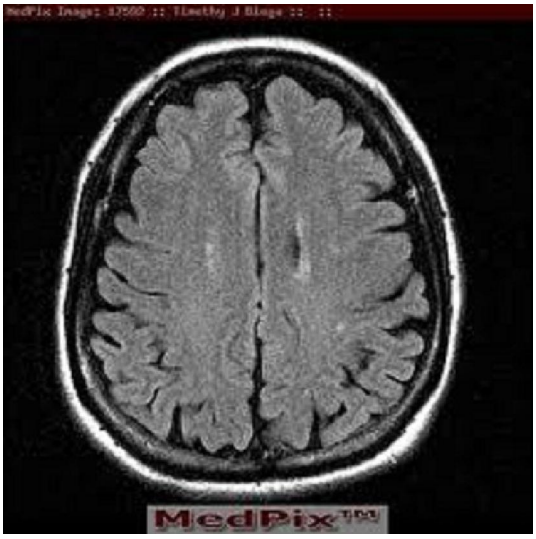

c

d

e

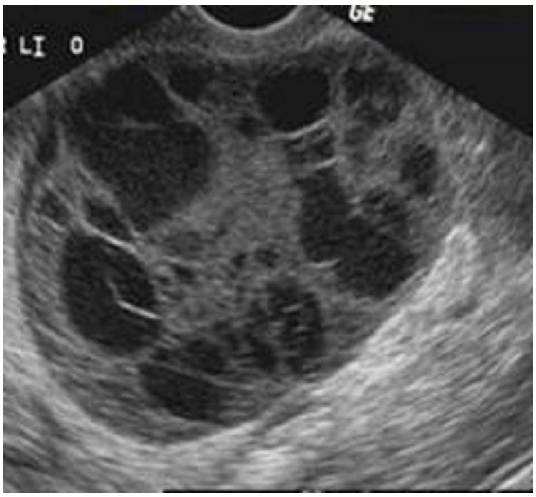

f

g

Figure 7. Host Images a) CT scan b) Mammogram c) MRA d) Nuclear e) PET f) Ultrasound g) X-ray

We have implemented system in the CT-SVD and SVD domains with the host images of size 512x512 shown in Figure 7 a) - g) and the watermark image in Figure 4(b) with Matlab12 software. For implementation in CT-SVD domain, initially we have subjected the host images to 1 level contourlet decomposition. The LF band of size 256x256 is divided into non overlapping blocks assuming *bxb*=2x2. This gives a block space of 128x128. Similarly, we have implemented the algorithms in the SVD domain assuming *bxb*=4x4. Accordingly, the host image is divided into 128x128 non overlapping blocks each size 4x4. Rest of the assumptions is same for both the domains. We have made the assumptions, $k_i = 64$, $k_j = 64$, i.e., $k = (64,64)$ and $n = 6$. By 6 iterations of Arnold Transform, k is mapped to (127,62). For the watermark bit W_{11}, the block (127,62) is selected out of the 128x128 block space and SVD is applied on that and I_1, I_2 and I_3 are computed for the diagonal matrix. The sign bit sequence of these invariants is the Master Share for W_{11}. Similarly, the Master Share is created for the rest of the watermark bits by incrementing both k_i and k_j by 1. The Secret Share is created by a XOR operation on the Master Share and the corresponding scrambled watermark bits. Similarly on extraction, the Master Share is created for the host image and it is XORed with the corresponding Secret Share to reveal the scrambled watermark.

We have evaluated the performance of our algorithm with Bit Error Rate (BER), Normalized Correlation Coefficient (NC), Structural Similarity Index Measure (SSIM) and Universal Image Quality Index (UIQI) metrics. These performance metrics show that, the watermarks constructed are intact for all modalities as shown in Figure 8.

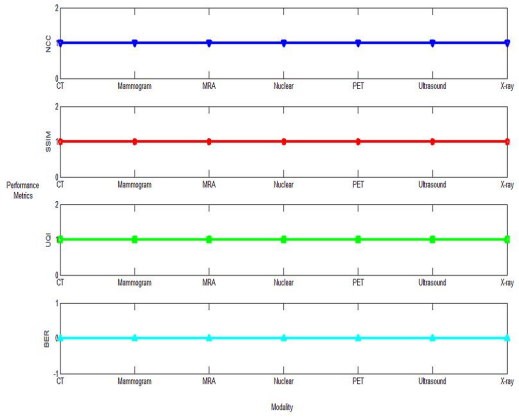

Figure 8. Performanace Metrics - Watermark Construction from Unattacked Host Images

We have evaluated the performance of the system under noise attacks for all the modalities in both the domains. We have generated the attacked host images by adding AWGN, poisson, salt and pepper and speckle noise with Matlab 12 software. AWGN is added for values of SNR ranging from 1db to 10 dB in increments of 1dB resulting in 10 attacked images under each modality. Similarly, poisson noise is added to each of the host images to generate 1 attacked image from each. Salt and Pepper Noise is added in increments of.05 from.05 to 1 resulting in 20 attacked images in each modality. Speckle noise is added in increments of.04 from.04 to 1, resulting in 25 attacked images for each modality. We evaluate the robustness of the watermarks and thus the system with the NC values and the readability of the watermarks with the Zxing decoder. We have tabulated the NC values of the watermarks extracted from these images and their readability in Table 1, Table 2, Table 3 and Table 4 for AWGN, poisson, salt & pepper and speckle noise attacks respectively. We have given the readability within parentheses in binary i.e., '0' for watermarks not recognized by the decoder and '1' watermarks decodable into HL7 messages. From the tables we can see that the NC values are closer to unity in both the domains. However, we can also see that, many watermarks are not decodable in spite of similarity to the original watermark. This can be attributed to the loss of significant data required for error correction. Watermarks not recognized by decoders under AWGN attacks in both domains are shown in Figure 9.

From Tables 1to IV, we understand that the system behaves consistently in the CT-SVD domain. The system provides robustness against the four noise attacks for all modalities and noise parameters, except for mammograms in the CT-SVD domain. In the SVD domain, the system provides robustness to only CT, PET and Ultrasound images against AWGN attacks. We can see that only the watermarks extracted from attacked nuclear image with 1dB and 2dB SNR are not readable. Like in CT-SVD domain, we can see that watermarks extracted from mammograms do not withstand any of the noise attacks from the lowest to the highest intensities. In addition to mammograms, attacked MRA and X-Ray images are also vulnerable to AWGN attacks.

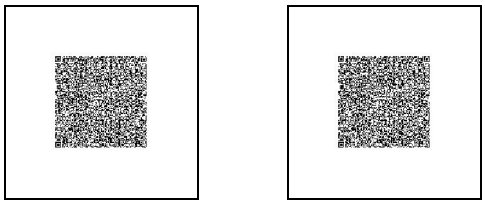

(a) (b)

Figure 9. Undecodable Watermarks a) CT-SVD b) SVD

We also understand that the mammogram and MRA images are not robust under poisson attacks in the SVD domain. We can see that the system behaves similarly in both the domains for salt and pepper attacks invariably from the smallest to highest noise densities. Our experimental results show that under salt and pepper noise attacks, the NC values are uniform for all image modalities, for all noise densities in both domains. Under speckle noise attacks, the robustness of the system is not consistent for MRA images in SVD domain, i.e., watermarks extracted from few attacked images with higher variances are robust. The computational times of embedding and extraction algorithms in both the domains are shown in Figure 10. Surprisingly, the algorithms in the CT-SVD domain have better computational efficiency in spite of the time taken for contourlet decomposition.

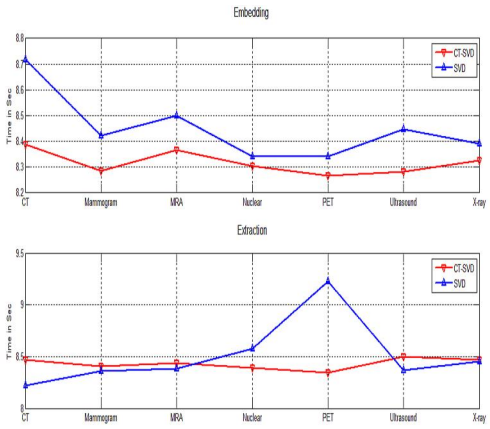

Figure 10. Computational Complexity

6. Discussion

From the underlying principles of zero-watermarking, it is apparent that the robustness to attacks depends upon the stability of the Master Share. From the experimental results, we find that the proposed system offers better robustness in the CT-SVD domain when compared to the SVD domain. We have observed under all the noise attacks, there is a change in the invariant I_1 with complete sign reversal for majority of blocks for all noise densities in the both the domains, Hence, the Master Shares constructed from the attacked images vary from the original ones, leading to imperfect watermark construction. From literature, we understand that I_1 is the moment of inertia of an image around its centroid where the pixel intensities are same as physical density. We have shown the differences in Master Share between attacked and unattacked host images under all attacks for selected parameters in Table 5. We can see that, the differences are highly pronounced in the SVD domain. Though the differences follow the same pattern, the variations are confined to smaller regions in CT-SVD domain and scattered over large regions in the SVD domain. Classical watermarking systems demand the intactness of the extracted watermarks sufficient to be recognized for authentication or copyright protection applications. However, QR code based systems have a stringent requirement that the watermarks must be decodable by a QR code scanner. The robustness of the proposed system to highly intensive noise attacks is attributed to the Hu's invariants and the stability of the SVs.

We have shown that robustness can be achieved with three lower order Hu's invariant moments, instead of the entire set of seven invariants. The security of the proposed system is determined with these parameters: number of levels of contourlet decomposition, the size of the partitioned blocks, initial block selection and the number of iterations for Arnold Transform. The proposed system offers good degree of freedom to select these parameters within the permissible space. For example, the number of levels of contourlet decomposition and the size of the partitioned blocks depends upon the size of the watermark. In the proposed system, we have chosen these parameters such that the embedding block space is 128x128. Further, the initial block selection offers freedom to select any arbitrary block within this space. Above all, the number of iterations of the Arnold Transform determines the synchronization of the watermark.

It is evident that any attempt to compromise the proposed system requires the adversary to know the exact values of these parameters. It would be highly unrealistic to determine the value of these parameters with a blind brute force attack due to the computational complexities. Further, another level of security can be added by permuting I_1, I_2 and I_3 for Master Share creation.

However, we have observed that the proposed system is not robust with mammogram images in both the domains for all the noise attacks. This is attributed to the nature of the image we have taken. Black pixels are predominant in the left half of our mammogram image due to which, the entire set of invariant moments of the partitioned blocks in this region are zeros. These moments get altered due to the introduction of noise and hence, the Master Shares differ for and unattacked images leading to imprecise watermark construction. Hence, it is required to formulate new approaches to counter this issue in medical images with small regions of interest. As an alternative, only the region of interest can be iteratively considered in computing the Master Share to achieve robustness.

7. Conclusion

In this paper, we have proposed a zero-watermarking system to embed a HL7 message in the form of a QR code for medical image authentication and improved radiology readings. The proposed system is implemented and tested in the CT-SVD and SVD domains. From the experimental results, we find that the composite CT-SVD domain provides better robustness to noise attacks rampant in medical images. The simplicity of the proposed system, its robustness, security and the infiltration of smart phones enabled with QR code readers imply the practicability of deploying the system in healthcare institutions to provide better care to remote destinations deprived of in-house radiologists. The proposed system can be improved by identifying alternate transforms and their combinations for Master Share creation. This paper signifies the need to carry out further research to identify invariants in medical images with smaller regions of interest which are highly vulnerable to attacks.

Acknowledgement

We acknowledge Richard Wheeler for granting us permission to illustrate the structure of the QR code.

Corresponding Author

R. Velumani
Associate Professor –IT
Sethu Institute of Technology
Pullor, Kariapatti-India 626115.
Email: velumaniramesh@yahoo.com

References

1. Benjamin M, Aradi Y, Shreiber R. From shared data to sharing workflow: Merging PACS and

teleradiology, European Journal of Radiology 2010; 73(1): 3-9.
2. Benvon Cramer, Gregory Butler, Jean Chalaoui, Kelly Silverthorn, Luigi Lepanto David Koff. CAR standards for Teleradiology 2008 http://www.car.ca/uploads/standards%20guidelines/Standard_Teleradiology_EN.pdf, Accessed October 2012.
3. The Health Insurance Portability and Accountability Act (HIPAA), http://www.hhs.gov/ocr/privacy/index.html, Accessed October 2012.
4. Nyeem H, Boles W, Boyd C. A Review of Medical Image Watermarking Requirements for Teleradiology. Journal of Digital Imaging (Springer-Verlag), 2012; 1-18.
5. Denso-Wave., http://www.denso-wave.com/qrcode/index-e.html , Accessed October 2012.
6. Chang C, Hwang K. F., Hwang M. S. A block based digital watermarks for copy protection of images, In Proc. of the 5th Asia-Pacific Conference on Communications Beijing, China 1999; vol. 2: 977–980.
7. Naor M., Shamir A. Visual cryptography, In Proc. of the Advances in Cryptology—EUROCRYPT'94, Lecture Notes in Computer Science (Springer-Verlag) 1995; 950: pp.1–12.
8. Guo H., Georganas N. D. A novel approach to digital image watermarking based on a generalized secret sharing scheme. Multimedia Systems 2003; 9(3):249-260.
9. Chang C., Chuang J. C. An image intellectual property protection scheme for gray-level images using visual secret sharing strategy, Pattern Recognition Letters 2002, 23(8):931–941.
10. Richard J. Prokop, Anthony P. Reeves A survey of moment-based techniques for unoccluded object representation and recognition, CVGIP: Graphical Models and Image Processing 1992 Vol. 54(5): pp.438-460.
11. HL7 OBX – Observation Segment, http://www.corepointhealth.com/resource-center/hl7-resources/hl7-obx-segment, Accessed December 2012.
12. Tan Jin Soon. QR Code. Synthesis Journal 2008; section. http://www.itsc.org.sg/pdf/synthesis08/Three_QR_Code.pdf. Accessed October 2012.
13. García-Betances R. I., Huerta M. K. A Review of Automatic Patient Identification Options for Public Health Care Centers with Restricted Budgets, Online Journal of Public Health Informatics 2012 (4), No. 1.
14. Kerry Davis, Emergency workers scan QR codes to quickly access health information, http://www.pcworld.com/article/256550/emergency_workers_scan_qr_codes_to_quickly_access_health_information.html. Accessed June 2012.
15. Chen WY, Wang JW. Nested image steganography scheme using QR-barcode technique, Optical Engineering 2009; (48): No. 5, 057004.
16. Kim J, Kim N, Lee D, Park S, Lee S, Watermarking two dimensional data object identifier for authenticated distribution of digital multimedia contents. Signal Processing: Image Communication, 2010; 25(8): 559-576.
17. Cordos A, Orza B, Vlaicu A, Meza S, Avram C, Petrovan B. Hospital Information System using HL7 and DICOM standards. WSEAS transactions on information science and applications 2010; Vol.7: 1295-1304.
18. Do MN, Vetterli M. The contourlet transform: an efficient directional multiresolution image representation. IEEE Transactions on Image Processing 2005; 14(12):2091-2106.
19. Salahi E, Moin MS, Salahi A. A new visually imperceptible and robust image watermarking scheme in Contourlet domain 2008; In Proceedings of IEEE International Conference on Intelligent Information Hiding and Multimedia Signal Processing:457-460.
20. Shu Z, Wang S, Deng C, Liu G, Zhang L. Watermarking algorithm based on contourlet transform and human visual model 2008; In Proc. of IEEE International Conference on Embedded Software and Systems:348-352.
21. Song H, Yu S, Yang X, Song L, Wang C. Contourlet-based image adaptive watermarking. Signal Processing: Image Communication, 2008;23(3):162-178.
22. Zeng FJ, Zhou AM. Image zero-watermarking algorithm based on Contourlet transform and singular value decomposition. Journal of Computer Applications 2008;28(8): pp.2033-2035.
23. Hsu S, Hou YC, Copyright protection scheme for digital images using visual cryptography and sampling methods, Optical engineering, 2005;44(7):077003-077003.
24. Wang MS, Chen WC, A hybrid DWT-SVD copyright protection scheme based on k-means clustering and visual cryptography, Computer Standards & Interfaces 2009;31(4): 757-762.
25. Rawat S, Raman B, A blind watermarking algorithm based on fractional Fourier transform and visual cryptography. Signal Processing 2012;92(6):1480-1491.

26. Fan TY, Chieu BC, Chao HC. Robust copyright-protection scheme based on visual secret sharing and Bose–Chaudhuri–Hocquenghem code techniques. Journal of Electronic Imaging 2012; 21(4):043018-043018.
27. Hu MK. Visual pattern recognition by moment invariants. IRE Transactions on Information Theory 1962;8(2):179-187.
28. Huang Z, Leng J. Analysis of Hu's moment invariants on image scaling and rotation. In 2nd IEEE International Conference on Computer Engineering and Technology (ICCET) 2010; Vol. 7, pp. V7-476.
29. Alghoniemy M, Tewfik AH. Image watermarking by moment invariants. In Proceedings of International Conference on Image Processing 2000; Vol. 2:73-76.
30. Alghoniemy M, Tewfik AH. Geometric invariance in image watermarking. IEEE Transactions on Image Processing, 2004;13(2):145-153.
31. Tzouveli P, Ntalianis K, Kollias S. Video object watermarking using Hu moments. In Proceedings of 13th International Conference on Systems, Signals and Image Processing, Budapest, Hungary 2006; p.6.
32. Mahbuba Ferdous, Mahmuda Ferdous, Uddin MS. Invisible Watermarking Technique for Copyright Protection, Journal of Imaging and Vision Research 2012; Vol.1, No. 2:2-6.
33. Li XW, Cho SJ, Kim ST, 2-D CAT-Based medical image watermarking algorithm, International Journal of Computer Theory and Engineering 2012, Vol.4, No. 5:722-725.
34. Liu G, Liu H, Kadir A. Wavelet-based color pathological image watermark through dynamically adjusting the embedding intensity. Computational and Mathematical Methods in Medicine vol. 2012; Article ID 406349.
35. Lal S, Chandra M, Upadhyay GK, Gupta D. Removal of Additive Gaussian Noise by Complex Double Density Dual Tree Discrete Wavelet Transform. MIT International Journal of Electronics and Communication Engineering 2011; 1(1): 8-16.
36. Sawatzky A, (Nonlocal) total variation in medical imaging, Ph.D. dissertation, Institute for Computational and Applied Mathematics, University of Münster, 2011.
37. Rafael C. Gonzalez, Richard E. Woods. *Digital Image processing using MATLAB*, Second Edition, Mc Graw hill 2005.
38. Zxing, http://code.google.com/p/zxing/, Accessed October 2012.

Table 1 NC and Readability under AWGN Attacks

SNR in dB	Modality							
	Domain	CT	Mammogram	MRA	Nuclear	PET	Ultrasound	X-ray
1		0.9989(1)	0.9930(0)	0.9989(1)	0.9988(1)	0.9989(1)	0.9993(1)	0.9990(1)
	CT-SVD	0.9988(1)	0.9908(0)	0.9965(0)	0.9960(0)	0.9989(1)	0.9991(1)	0.9967(0)
2	SVD	0.9990(1)	0.9928(0)	0.9989(1)	0.9986(1)	0.9994(1)	0.9993(1)	0.9988(1)
	CT-SVD	0.9989(1)	0.9912(0)	0.9965(0)	0.9974(0)	0.9988(1)	0.9991(1)	0.9966(0)
3	SVD	0.9989(1)	0.9929(0)	0.9989(1)	0.9986(1)	0.9994(1)	0.9991(1)	0.9988(1)
	CT-SVD	0.9987(1)	0.9912(0)	0.9962(0)	0.9972(1)	0.9988(1)	0.9992(1)	0.9965(0)
4	SVD	0.9989(1)	0.9922(0)	0.9989(1)	0.9989(1)	0.9995(1)	0.9992(1)	0.9987(1)
	CT-SVD	0.9989(1)	0.9905(0)	0.9964(0)	0.9978(1)	0.9989(1)	0.9991(1)	0.9968(0)
5	SVD	0.9988(1)	0.9922(0)	0.9988(1)	0.9990(1)	0.9993(1)	0.9992(1)	0.9985(1)
	CT-SVD	0.9987(1)	0.9911(0)	0.9964(0)	0.9979(1)	0.9987(1)	0.9991(1)	0.9966(0)
6	SVD	0.9986(1)	0.9924(0)	0.9987(1)	0.9989(1)	0.9994(1)	0.9991(1)	0.9988(1)
	CT-SVD	0.9991(1)	0.9916(0)	0.9960(0)	0.9977(1)	0.9988(1)	0.9991(1)	0.9965(0)
7	SVD	0.9985(1)	0.9926(0)	0.9985(1)	0.9990(1)	0.9995(1)	0.9991(1)	0.9988(1)
	CT-SVD	0.9989(1)	0.9910(0)	0.9964(0)	0.9981(1)	0.9988(1)	0.9992(1)	0.9967(0)
8	SVD	0.9985(1)	0.9926(0)	0.9985(1)	0.9990(1)	0.9995(1)	0.9992(1)	0.9985(1)
	CT-SVD	0.9988(1)	0.9913(0)	0.9961(0)	0.9982(1)	0.9988(1)	0.9991(1)	0.9963(0)
9	SVD	0.9987(1)	0.9923(0)	0.9985(1)	0.9990(1)	0.9994(1)	0.9991(1)	0.9989(1)
	CT-SVD	0.9988(1)	0.9909(0)	0.9959(0)	0.9983(1)	0.9987(1)	0.9992(1)	0.9966(0)
10	SVD	0.9984(1)	0.9914(0)	0.9985(1)	0.9991(1)	0.9995(1)	0.9990(1)	0.9989(1)
	CT-SVD	0.9989(1)	0.9912(0)	0.9960(0)	0.9981(1)	0.9988(1)	0.9992(1)	0.9967(0)

Table 2 NC and Readability under Poisson Noise Attacks

Domain	Modality						
	CT	Mammogram	MRA	Nuclear	PET	Ultrasound	X-ray
CT-SVD	0.9991(1)	0.9927(0)	0.9991(1)	0.9971(1)	0.9996(1)	0.9987(1)	0.9992(1)
SVD	0.9994(1)	0.9866(0)	0.9973(0)	0.9988(1)	0.9992(1)	0.9977(1)	0.9983(1)

Table 3 NC and Readability under Salt and Pepper Noise Attacks

Noise Density	Domain	Modality						
		CT	Mammogram	MRA	Nuclear	PET	Ultrasound	X-ray
0.1	CT-SVD	0.9991(1)	0.9928(0)	0.9995(1)	0.9971(1)	0.9998(1)	0.9987(1)	0.9993(1)
	SVD	0.9994(1)	0.9875(0)	0.9984(0)	0.9987(1)	0.9994(1)	0.9977(1)	0.9989(1)
0.2	CT-SVD	0.9991(1)	0.9928(0)	0.9995(1)	0.9971(1)	0.9998(1)	0.9987(1)	0.9993(1)
	SVD	0.9994(1)	0.9875(0)	0.9984(0)	0.9987(1)	0.9994(1)	0.9977(1)	0.9989(1)
0.3	CT-SVD	0.9991(1)	0.9928(0)	0.9995(1)	0.9971(1)	0.9998(1)	0.9987(1)	0.9993(1)
	SVD	0.9994(1)	0.9875(0)	0.9984(0)	0.9987(1)	0.9994(1)	0.9977(1)	0.9989(1)
0.4	CT-SVD	0.9991(1)	0.9928(0)	0.9995(1)	0.9971(1)	0.9998(1)	0.9987(1)	0.9993(1)
	SVD	0.9994(1)	0.9875(0)	0.9984(0)	0.9987(1)	0.9994(1)	0.9977(1)	0.9989(1)
0.5	CT-SVD	0.9991(1)	0.9928(0)	0.9995(1)	0.9971(1)	0.9998(1)	0.9987(1)	0.9993(1)
	SVD	0.9994(1)	0.9875(0)	0.9984(0)	0.9987(1)	0.9994(1)	0.9977(1)	0.9989(1)
0.6	CT-SVD	0.9991(1)	0.9928(0)	0.9995(1)	0.9971(1)	0.9998(1)	0.9987(1)	0.9993(1)
	SVD	0.9994(1)	0.9875(0)	0.9984(0)	0.9987(1)	0.9994(1)	0.9977(1)	0.9989(1)
0.7	CT-SVD	0.9991(1)	0.9928(0)	0.9995(1)	0.9971(1)	0.9998(1)	0.9987(1)	0.9993(1)
	SVD	0.9994(1)	0.9875(0)	0.9984(0)	0.9987(1)	0.9994(1)	0.9977(1)	0.9989(1)
0.8	CT-SVD	0.9991(1)	0.9928(0)	0.9995(1)	0.9971(1)	0.9998(1)	0.9987(1)	0.9993(1)
	SVD	0.9994(1)	0.9875(0)	0.9984(0)	0.9987(1)	0.9994(1)	0.9977(1)	0.9989(1)
0.9	CT-SVD	0.9991(1)	0.9928(0)	0.9995(1)	0.9971(1)	0.9998(1)	0.9987(1)	0.9993(1)
	SVD	0.9994(1)	0.9875(0)	0.9984(0)	0.9987(1)	0.9994(1)	0.9977(1)	0.9989(1)
1	CT-SVD	0.9991(1)	0.9928(0)	0.9995(1)	0.9971(1)	0.9998(1)	0.9987(1)	0.9993(1)
	SVD	0.9994(1)	0.9875(0)	0.9984(0)	0.9987(1)	0.9994(1)	0.9977(1)	0.9989(1)

Table 4 NC and Readability under Speckle Noise Attacks

Variance	Domain	Modality						
		CT	Mammogram	MRA	Nuclear	PET	Ultrasound	X-ray
.04	CT-SVD	0.9991(1)	0.9934(0)	0.9985(1)	0.9971(1)	0.9996(1)	0.9987(1)	0.9991(1)
	SVD	0.9994(1)	0.9886(0)	0.9969(1)	0.9988(1)	0.9991(1)	0.9977(1)	0.9983(1)
0.12	CT-SVD	0.9991(1)	0.9927(0)	0.9988(1)	0.9971(1)	0.9997(1)	0.9987(1)	0.9993(1)
	SVD	0.9994(1)	0.9872(0)	0.9972(1)	0.9988(1)	0.9992(1)	0.9977(1)	0.9984(1)
0.2	CT-SVD	0.9991(1)	0.9928(0)	0.9991(1)	0.9971(1)	0.9998(1)	0.9987(1)	0.9991(1)
	SVD	0.9994(1)	0.9867(0)	0.9971(0)	0.9988(1)	0.9992(1)	0.9977(1)	0.9984(1)
0.28	CT-SVD	0.9991(1)	0.9928(0)	0.9991(1)	0.9971(1)	0.9997(1)	0.9987(1)	0.9993(1)
	SVD	0.9994(1)	0.9866(0)	0.9976(1)	0.9988(1)	0.9992(1)	0.9977(1)	0.9983(1)
0.36	CT-SVD	0.9991(1)	0.9928(0)	0.9991(1)	0.9971(1)	0.9997(1)	0.9987(1)	0.9994(1)
	SVD	0.9994(1)	0.9867(0)	0.9975(0)	0.9988(1)	0.9992(1)	0.9977(1)	0.9984(1)
0.44	CT-SVD	0.9991(1)	0.9928(0)	0.9991(1)	0.9971(1)	0.9997(1)	0.9987(1)	0.9994(1)
	SVD	0.9994(1)	0.9868(0)	0.9977(0)	0.9988(1)	0.9992(1)	0.9977(1)	0.9985(1)
0.52	CT-SVD	0.9991(1)	0.9927(0)	0.9991(1)	0.9971(1)	0.9997(1)	0.9987(1)	0.9993(1)
	SVD	0.9994(1)	0.9869(0)	0.9977(1)	0.9988(1)	0.9992(1)	0.9977(1)	0.9983(1)
0.6	CT-SVD	0.9991(1)	0.9928(0)	0.9991(1)	0.9971(1)	0.9997(1)	0.9987(1)	0.9994(1)
	SVD	0.9994(1)	0.9871(0)	0.9978(0)	0.9988(1)	0.9992(1)	0.9977(1)	0.9985(1)
0.68	CT-SVD	0.9991(1)	0.9928(0)	0.9991(1)	0.9971(1)	0.9996(1)	0.9987(1)	0.9993(1)
	SVD	0.9994(1)	0.9872(0)	0.9981(0)	0.9988(1)	0.9993(1)	0.9977(1)	0.9986(1)
0.76	CT-SVD	0.9991(1)	0.9928(0)	0.9991(1)	0.9971(1)	0.9997(1)	0.9987(1)	0.9993(1)
	SVD	0.9994(1)	0.9872(0)	0.9978(0)	0.9988(1)	0.9993(1)	0.9977(1)	0.9986(1)
0.84	CT-SVD	0.9991(1)	0.9928(0)	0.9991(1)	0.9971(1)	0.9996(1)	0.9987(1)	0.9993(1)
	SVD	0.9994(1)	0.9873(0)	0.9978(1)	0.9988(1)	0.9992(1)	0.9977(1)	0.9985(1)
0.92	CT-SVD	0.9991(1)	0.9928(0)	0.9991(1)	0.9971(1)	0.9997(1)	0.9987(1)	0.9993(1)
	SVD	0.9994(1)	0.9875(0)	0.9981(0)	0.9988(1)	0.9992(1)	0.9977(1)	0.9986(1)
1	CT-SVD	0.9991(1)	0.9928(0)	0.9992(1)	0.9971(1)	0.9997(1)	0.9987(1)	0.9993(1)
	SVD	0.9994(1)	0.9873(0)	0.9981(1)	0.9988(1)	0.9992(1)	0.9977(1)	0.9983(1)

Table 5 Differences in Master Share

Attack	Domain	Modality						
		CT	Mammogram	MRA	Nuclear	PET	Ultrasound	X-ray
AWGN SNR: 1 dB	CT-SVD		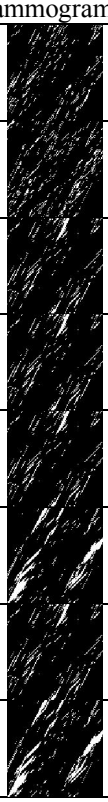					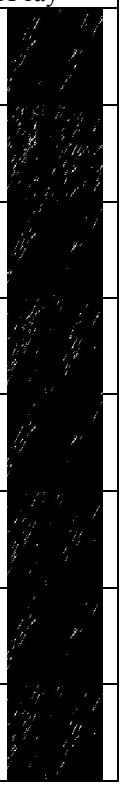
	SVD							
Poisson	CT-SVD							
	SVD							
Salt & Pepper Noise Desnity:1	CT-SVD							
	SVD							
Speckle Variance:.8	CT-SVD							
	SVD							

7/25/2018